Environmental Science & Technology Letters

Letter

Cite This: Environ. Sci. Technol. Lett. 2018, 5, 366−371

pubs.acs.org/journal/estlcu

Photodegradation of Secondary Organic Aerosol Material Quantified with a Quartz Crystal Microbalance

Kurtis T. Malecha, Zicheng Cai, and Sergey A. Nizkorodov*

Department of Chemistry, University of California, Irvine, California 92697-2025, United States

Supporting Information

ABSTRACT: We used a quartz crystal microbalance (QCM) to quantify the mass loss resulting from exposure of secondary organic aerosol (SOA) particles deposited on the QCM crystal to 254, 305, and 365 nm radiation. We coupled the QCM setup to a proton transfer reaction time-of-flight mass spectrometer (PTR-ToF-MS) to chemically resolve the photoproduced volatile organic compounds (VOCs) responsible for the mass loss. The photoproduced VOCs detected by the PTR-ToF-MS accounted for ∼50% of the mass loss rates measured with the QCM. Weakly absorbing SOA produced by ozonolysis of α-pinene or d-limonene exhibited a much larger mass loss rate in both the QCM and the PTR-ToF-MS data compared to that of strongly absorbing SOA produced by photooxidation of guaiacol. We predict that the fractional mass loss rate of α-pinene ozonolysis SOA should be as high as ∼1%/h on the summer solstice in Los Angeles in the lower troposphere and ∼4%/h in the stratosphere. The mass loss rates for SOA particles crossing a typical 254 nm oxidation flow reactor, which is routinely used for rapid aging of organic aerosol particles, are expected to be negligible because of the short residence time inside the reactor.

INTRODUCTION

Secondary organic aerosol (SOA) represents a complex mixture of a large number of products of photooxidation of volatile organic compounds (VOCs).[1] The least volatile SOA compounds condense into particles, which affect the climate by scatting and absorbing solar radiation and by modifying cloud properties.[2] Photodegradation of condensed-phase material in SOA has recently been shown to occur on atmospherically relevant time scales.[3−9] These photodegradation processes tend to break chemical bonds in SOA compounds, leading to smaller and therefore more volatile products, which can more easily evaporate from SOA particles. However, all the previous experimental observations of SOA photodegradation have been qualitative, and at best, they reported only rough estimates for the rate of SOA photodegradation. For example, in our previous study, we could only estimate a lower limit of >1% mass loss per day for the photodegradation rate of SOA particles produced from common VOCs.[3] That study relied on a proton transfer reaction time-of-flight mass spectrometer (PTR-ToF-MS) to observe small, oxygenated VOC products (OVOCs) of SOA photodegradation, such as acetone, formic acid, acetic acid, and acetaldehyde, and likely missed volatile compounds that the PTR-ToF-MS cannot detect such as saturated hydrocarbons, CO, and CO_2.[10]

The contribution of condensed-phase photochemistry to aging of SOA particles in oxidation flow reactors (OFRs) is also uncertain. OFRs are increasingly used to achieve an equivalent of days or even weeks of atmospheric processing in seconds by exposing SOA to very high mixing ratios of OH.[11] OFRs rely on strong 254 or 185 nm radiation to produce a high concentration of OH inside the reactor. This high concentration of radicals leads to functionalization followed by fragmentation of the molecules in particles.[12] In parallel with this fragmentation, direct photolysis of the SOA compounds may be possible. The effect of photolysis has been extensively modeled but has not been systematically tested by experiments.[13,14]

In this work, we are using a quartz crystal microbalance (QCM) to directly measure submicrogram mass changes during photodegradation of SOA particles deposited on an inert substrate in real time. The powerful combination of QCM measurements with the PTR-ToF-MS analysis of the volatile OVOC photoproducts makes it possible to probe the chemical mechanisms for SOA undergoing photodegradation. The QCM has a rich history of applications in atmospheric chemistry, for example, in studying SOA material evaporation rates,[15] the extent of water absorption on aerosols,[16−19] oxidative aging of organics,[20] and photosensitized processes.[21] Our measurements demonstrate the utility of QCM for aerosol photodegradation experiments and make it possible to quantify photodegradation rates of SOA at different wavelengths, including the 254 nm radiation used in OFRs as well as 305 and 365 nm radiation

Received: April 28, 2018
Revised: May 15, 2018
Accepted: May 15, 2018
Published: May 15, 2018

DOI: 10.1021/acs.estlett.8b00231
Environ. Sci. Technol. Lett. 2018, 5, 366−371

relevant in tropospheric photochemistry. We show that photodegradation readily occurs on SOA derived from α-pinene and d-limonene ozonolysis. In contrast, guaiacol/high-NO_x SOA is found to be more photoresistant despite being more light-absorbing. Our results support the conclusion that condensed-phase photochemistry can lead to measurable mass loss from SOA particles on time scales of hours, thus counteracting the aerosol particle growth from gas-to-particle partitioning.

MATERIALS AND METHODS

The SOA was generated by oxidation of selected VOCs in either a smog chamber or an aerosol flow tube. Three different types of SOA were investigated for this study: α-pinene ozonolysis (APIN/O_3), d-limonene ozonolysis (LIM/O_3), and guaiacol high-NO_x photooxidation (GUA/NO_x). The ozonolysis experiments were performed in a flow tube, and the high-NO_x experiments were performed in a smog chamber with the same procedures and conditions as previously reported.[3,22] All SOA samples were prepared in at least triplicate. The SOA particles were collected using a Micro Orifice Uniform Deposit Impactor (MOUDI; MSP Corp. model 110-R) for 1−4 h with custom adapters to accommodate the 2.54 cm chrome/gold QCM crystals (Stanford Research Systems model O100RX1) as impaction substrates. The resulting SOA material collected on the QCM crystals was preconditioned under a flow of clean air overnight at 40 °C, to remove the more volatile compounds and allow the particles to merge in a continuous although not uniform film.[3] The masses collected ranged from 0.4 to 2.8 mg, as determined by weighing the crystal before and after the collection (and after preconditioning) with a Sartorius ME5-F balance (1 μg precision). Most of the material was distributed fairly evenly around the 2.54 cm crystal for each sample.

We modified a commercial QCM (Stanford Research Systems model QCM 200) holder to include a sealed space above the QCM crystal with a CaF_2 window on top. Details can be found in Figure S1. A flow of zero air (at 150 sccm) was sent through the space between the QCM crystal and the CaF_2 window, and a fraction of the outgoing air was then fed into a PTR-ToF-MS instrument (Ionicon model 8000) at 100 sccm. The PTR-ToF-MS was calibrated in the same manner described previously.[3]

Exposure to ultraviolet (UV) radiation reduced the mass of the SOA material remaining on the QCM crystal and increased its oscillation frequency. To convert the observed change in QCM frequency into SOA mass, a modified version of the Sauerbrey equation was used:[23]

$$\frac{dm}{dt} = -\frac{1}{C_f}\frac{df}{dt} \quad (1)$$

where df/dt is the rate of the frequency change during irradiation (in hertz per hour), C_f is the sensitivity factor (in hertz per microgram), and dm/dt is the mass change rate (in micrograms per hour). Because the collected particles did not form a completely uniform thin film (for which the Sauerbrey equation was developed) C_f had to be determined empirically for each sample. This was done by measuring the frequency for the clean crystal, collecting SOA on this crystal, determining the mass of SOA (Δm) collected by weighing it, and noting the frequency change (Δf) experienced by the QCM. The sensitivity factor was then calculated from eq 2 (the integrated form of eq 1).

$$C_f = -\frac{\Delta f}{\Delta m} \quad (2)$$

Typical sensitivity factors for these experiments ranged between 5 and 14 Hz/μg, with the theoretical sensitivity factor being 11.2 Hz/μg (more details are provided in the Supporting Information). The sensitivity factors were approximately independent of the QCM mass loading and the type of SOA at higher mass loadings (>1 mg on the crystal) but started to deviate from the theoretical sensitivity factor at lower mass loadings (Figure S2), presumably because there were not enough particles to form a continuous film on the surface.

The SOA material was irradiated directly on the QCM crystal with a suitable UV lamp. The lamps included a light-emitting diode (LED) centered at 305 nm (Thorlabs, Inc., model M300L4), another LED centered at 365 nm (Thorlabs, Inc., model M365LP1), and a mercury pen ray lamp centered at 254 nm (Spectronics Corp. model Spectroline 11SC-1). Using selected wavelengths of radiation as opposed to a full solar spectrum is standard practice in atmospheric photochemistry[24] because it provides information about the wavelength dependence of the process and avoids unnecessary heating of the sample with visible and near-infrared radiation, which does not initiate photodegradation processes. The wavelength dependence of the spectra of the lamps is shown in Figure S3. The incident power of each lamp was measured with a Coherent PS19Q power meter in the same geometry that was experienced by the QCM crystal. The resulting powers were 3.7, 2.5, and 13.8 mW for the 254, 305, and 365 nm lamps, respectively. With the 1 cm^2 area of the power meter, these correspond to spectral fluxes of radiation of 4.7×10^{15}, 3.8×10^{15}, and 2.5×10^{15} photons cm^{-2} s^{-1}, respectively. The 254 nm lamp has several emission lines from 250 to 380 nm (Figure S3), and the spectral flux of radiation due to the 254 nm emission line was 2.5×10^{15} photons cm^{-2} s^{-1}. We previously showed that power meter measurements agree reasonably well with actinometry experiments (not presented here).[3,25] The 254 nm spectral flux used in these experiments is comparable to that inside a typical OFR. For example, Li et al. noted that the spectral fluxes of radiation in their OFR were 2.0×10^{13} and 2.5×10^{15} photons cm^{-2} s^{-1} at 185 and 254 nm, respectively.[26]

The QCM crystals' masses were determined by direct weighing before and after collection of the SOA, but because of the design of the QCM sample holder and its o-rings, it was not possible to accurately determine the mass loss by weighing after the irradiation in the QCM holder. We relied on eq 1 instead to calculate the mass loss from the measured QCM frequency. The QCM measurements were acquired simultaneously with the PTR-ToF-MS measurements. The PTR-ToF-MS data were analyzed on the basis of a modified version of eq 2 from Malecha et al. to determine the mass loss rate based on the four quantified, photoproduced OVOCs (acetone, acetic acid, acetaldehyde, and formic acid).[3] Several controls were run for this study to make sure the observed mass loss is driven by SOA photochemistry, as described in the Supporting Information.

RESULTS AND DISCUSSION

Figure 1 shows results of a typical experiment in which the QCM frequency and selected OVOCs in the PTR-ToF-MS are observed during 254 nm irradiation of LIM/O_3 SOA. When the lamp is turned on, the QCM frequency starts to increase because the SOA material is losing mass from evaporation of

DOI: 10.1021/acs.estlett.8b00231
Environ. Sci. Technol. Lett. 2018, 5, 366−371

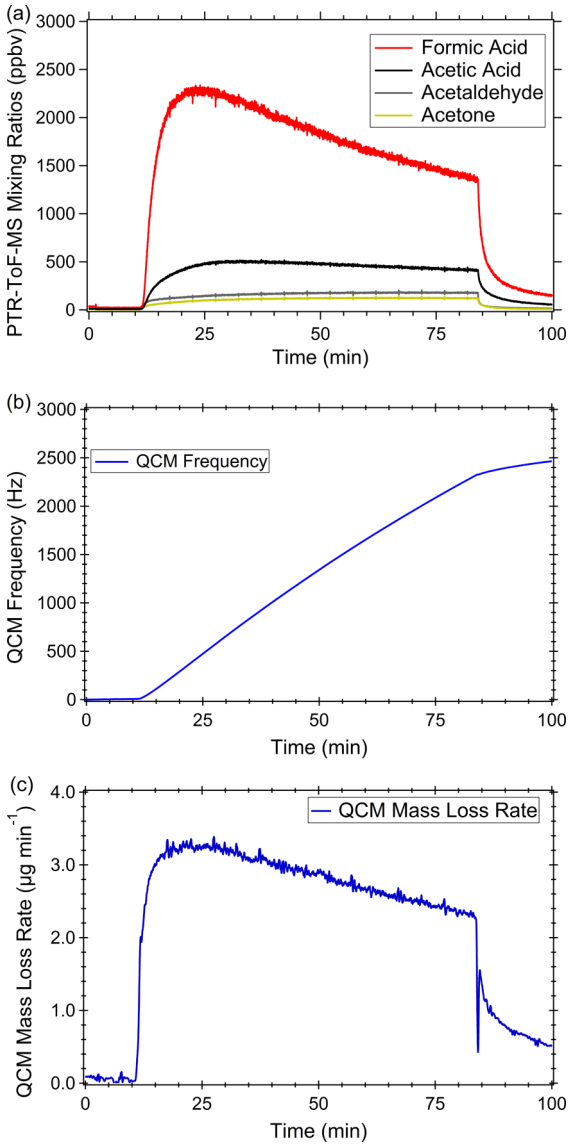

Figure 1. (a) Photoproduction of OVOCs observed during 254 nm irradiation of LIM/O_3 SOA. The lamp is turned on at ~10 min and turned off at ~85 min for this sample. (b) Baseline-corrected QCM frequency during irradiation. The frequency increases because the SOA material is losing mass. (c) QCM frequency's mass loss rate determined by taking the derivative of the frequency change with respect to time and then dividing by C_f (eq 1).

the OVOC photoproducts. The rate of mass loss from eq 1 is plotted in Figure 1c. The mass loss rate increases to a relatively constant value for ~15 min and then slowly decreases, replicating the measured trace of the major OVOC photoproduct, formic acid. When the lamp is turned off, the mass loss does not stop instantaneously because it takes some time for the OVOC photoproducts to diffuse out of the SOA material and escape in the gas phase.

In most experiments, the QCM frequency was observed to increase at a small constant rate even without radiation because of the slow evaporation of SOA material. To better visualize the extent of radiation-driven mass loss, the data shown in Figure 1 were baseline-corrected by subtracting the change attributable to evaporation (measured before the lamp was turned on):

$$f_{\text{corrected}}(t) = f(t) - \left(\frac{df}{dt}\right)_{\text{dark}} \times t \quad (3)$$

For the 254 and 305 nm experiments, the rate of change in the frequency due to SOA evaporation was much smaller than that due to photolysis. However, the much weaker effect of photolysis in 365 nm experiments would be difficult to ascertain without the baseline correction of eq 3.

The increase in the QCM frequency was accompanied by the photoproduction of a variety of OVOCs. The selected OVOCs plotted in Figure 1a include formic acid, acetic acid, acetaldehyde, and acetone, the same OVOCs that were shown to be produced during photodegradation in our previous studies.[3,25]

These observed changes in the PTR-ToF-MS traces and QCM frequency occurred readily for both 254 and 305 nm radiation; however, the baseline-subtracted 365 nm data, despite the larger photon flux, showed very small mass losses from both the PTR-ToF-MS and the QCM. This is consistent with photolysis yields and absorption cross sections of most molecules decreasing rapidly at longer wavelengths.[24,27]

The PTR-ToF-MS data were analyzed as described previously to calculate the mass loss rate attributable to OVOCs.[3] Briefly, the mass loss for each of the four major detected photoproducts (acetone, acetaldehyde, acetic acid, and formic acid) was calculated during the initial part of the photodegradation (e.g., ~20−30 min for the sample in Figure 1) using eq 2 from Malecha et al. and added together to calculate the total mass loss due to these photoproducts.[3] All data are presented in Table S1. As noted above, the mass loss is likely underpredicted by the PTR-ToF-MS because it is blind to compounds such as methane and carbon monoxide, which are known to be produced in photodegradation of SOA.[28] Figure 2 plots the estimated PTR-ToF-MS data versus the actual QCM mass loss rate. Despite the limitations of the PTR-ToF-MS approach, the data are reasonably correlated. Furthermore, these four OVOCs account for ~50% of the mass lost (based on the slope of Figure 2a).

The predominance of photoproducts containing just one or two carbon atoms forming during irradiation of APIN/O_3 and LIM/O_3 SOA suggests that the SOA compounds are cleaved by photolysis closer to the end portion of the molecule. This is consistent with the known mechanism of ozonolysis of these endocyclic monoterpenes, which produces a large number of products featuring an acetyl group [R-C(O)CH_3, such as pinonic acid, limononic acid, and their derivatives] or a formyl group [R-C(O)H, such as pinonaldehyde, limononaldehyde, and their derivatives]. We previously showed that Norrish type I and type II reactions can account for most of the products observed in photodegradation of LIM/O_3 SOA.[28] For example, Scheme 1 shows possible reactions in photolysis of limononaldehyde leading directly to acetone through a Norrish type II splitting and to formaldehyde, formic acid, acetaldehyde, and acetic acid by way of primary Norrish type I splitting followed by secondary cage reactions between free radicals (which are known to be present in irradiated SOA).[29] Limononaldehyde is too volatile to be present in SOA particles, but its more functionalized derivatives, which have lower vapor pressures, should still undergo photochemistry with a similar loss of C1 or C2 products. We note that this mechanism cannot be generalized to SOA formed from acyclic VOCs or to highly oxidized SOA compounds, which likely photolyze using more complicated mechanisms.

DOI: 10.1021/acs.estlett.8b00231
Environ. Sci. Technol. Lett. 2018, 5, 366−371

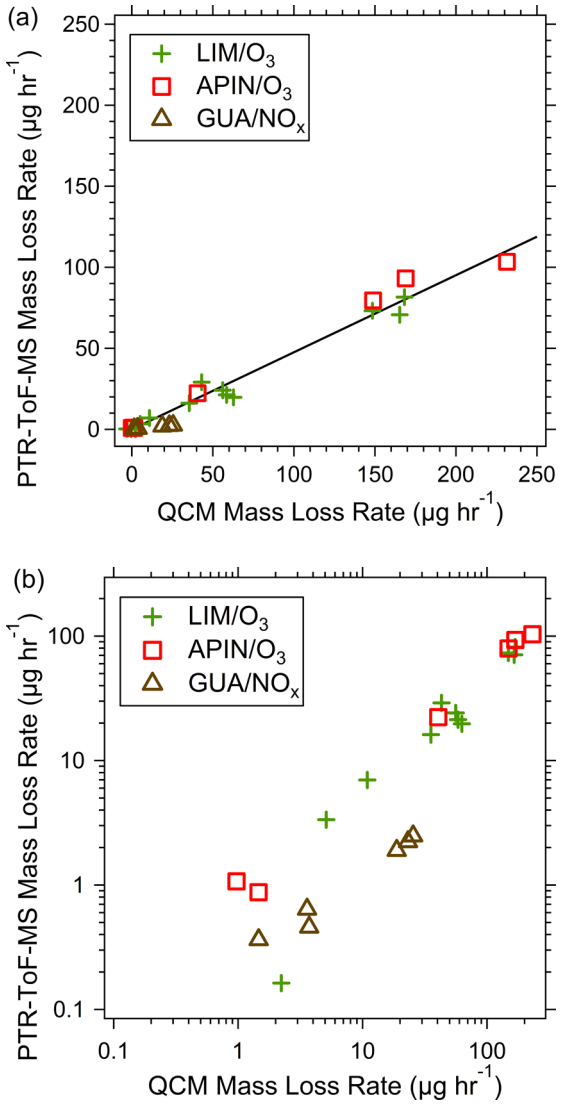

Figure 2. (a) QCM and PTR-ToF-MS mass loss rates are roughly proportional to one another for all SOA types in this study with the slope being ~0.5. The samples correspond to "LIM/O_3" = d-limonene/ozonolysis, "APIN/O_3" = α-pinene/ozonolysis, and "GUA/NO_x" = guaiacol (*o*-methoxyphenol)/high-NO_x photooxidation. (b) Log–log plot of the same data provided to zoom in on smaller values.

Scheme 1. Possible Reactions Involved in Photolysis of Limononaldehyde and Resulting in the Formation of Small OVOCs Observed by the PTR-ToF-MS

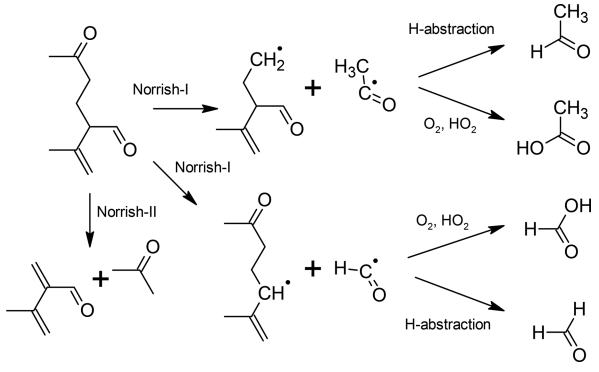

SOA produced from GUA is much more resilient to photolysis, suggesting a very different mechanism and confirming our previous observation that the mass loss rates are not correlated to the SOA absorption coefficients. Even though GUA/NO_x SOA has a mass absorption coefficient (~2 m^2/g) at 300 nm an order of magnitude higher than those of APIN/O_3 SOA and LIM/O_3 SOA (~0.05 m^2/g for both of them),[30] it has the lowest mass loss rate. The amount of OVOCs detected by the PTR-ToF-MS is close to the detection limit, and only a small mass loss rate is measured with the QCM. The resilience of guaiacol SOA to photodegradation suggests that its compounds must efficiently dispose of the electronic excitation energy. Many of these guaiacol/high-NO_x SOA products include derivatives of aromatic species such as nitrophenols, 4-nitroguaiacol, 6-nitroguaiacol, or 4,6-dinitroguaiacol, which have been detected in the condensed phase of the SOA particles.[31−33] Nitrophenols can undergo photolysis with quantum yields approaching unity in the gaseous phase, but the yields decrease to 10^{-4}–10^{-5} in the condensed phase.[34,35] The photoexcitation of nitrophenol clusters was shown to result in fast internal conversion mediated by intramolecular hydrogen bonding.[36] These studies suggest that GUA/NO_x SOA compounds may channel most of the excitation energy into heat by internal conversion in the condensed phase, thus slowing the photodegradation.

These measurements have several important implications. First, we can confirm that the particle mass loss driven by condensed-phase photochemistry is not a serious concern for most OFRs. It is well-known that heterogeneous oxidation in OFRs can significantly reduce the size and mass concentration of organic aerosol particles by fragmentation reactions.[12,37] However, with a 5 min residence time in an OFR reactor, <1% of the particle mass would be lost to the photodegradation processes investigated in this work. It is conceivable that a small fraction of the most photolabile molecules could still undergo photolysis or photoisomerization on this time scale, but these minority compounds would not strongly affect the overall particle mass concentration.

Second, the mass loss rates discussed in this work could be significant in the atmosphere. The measured fractional mass loss rate (FMLR) was in excess of 10%/h for the 254 nm irradiation and up to 4%/h for the 305 nm irradiation (Table S1). To estimate FMLR under atmospheric conditions, we assumed that it is proportional to the convolution of the spectral flux of radiation, $F(\lambda)$, and photodegradation efficiency, $E(\lambda)$.

$$\mathrm{FMLR} = \frac{1}{m}\frac{\mathrm{d}m}{\mathrm{d}t} = \int F(\lambda)E(\lambda)\,\mathrm{d}\lambda \tag{4}$$

We further assumed that $E(\lambda)$ drops exponentially with wavelength as suggested by our observations (see the Supporting Information for more details). With this approach, the FMLR values during the summer solstice in Los Angeles were found to be 3.8×10^{-6} s^{-1} for APIN/O_3 SOA at 0 km, 1.1×10^{-5} s^{-1} for APIN/O_3 SOA at 40 km, 6.2×10^{-6} s^{-1} for LIM/O_3 SOA at 0 km, and 1.6×10^{-5} s^{-1} for LIM/O_3 at 40 km. These rates would imply a ≤1% mass loss in 1 h in the troposphere and a 4% mass loss in 1 h in the stratosphere for the APIN/O_3 SOA. (These rates refer to the maximum flux one can expect during the summer solstice in Los Angeles and will be lower during other times of the day.) While this mass loss rate cannot compete with particle growth for ultrafine particles, which increase in diameter with an impressive rate exceeding 10

DOI: 10.1021/acs.estlett.8b00231
Environ. Sci. Technol. Lett. 2018, 5, 366−371

nm/h,[38] photodegradation processes can slow this growth for larger particles in the accumulation size mode, which dominates the overall mass loading of SOA in the atmosphere. This finding indirectly supports modeling conjecture by Hodzic et al.,[39] which predicted that SOA mass would decrease by 40−60% after 10 days of atmospheric aging if photolysis processes in particles are included in the model.

Third, these photodegradation processes are predicted to efficiently deplete organic particles from the stratosphere. Although SOA particles could potentially be transported to the stratosphere through deep convective transport,[40] the photodegradation processes described here would lead to their rapid loss. The aerosol particle viscosity would increase in these cool, dry areas of the atmosphere,[41] thus slowing diffusion in the particle and limiting the aging by heterogeneous reactions with OH to the particle surface. However, the photolysis-driven aging could still occur throughout the particle volume because UV radiation can penetrate deep inside the particle. It is remarkable that there does not appear to be a limit to the amount of SOA particle material that can be removed by photodegradation. For selected experiments, the APIN/O_3 particles were subjected to many days of continuous 254 nm irradiation. Nearly 100% of the mass was lost during this time for the APIN/O_3 sample (Figure S5); the QCM crystal had almost no visible traces of the organic film after the irradiation. The UV photodegradation is thus likely responsible for the small fraction of particulate organics above the tropopause, with only the most photostable organics surviving in this environment.[42]

■ ASSOCIATED CONTENT

Supporting Information

The Supporting Information is available free of charge on the ACS Publications website at DOI: 10.1021/acs.estlett.8b00231.

A drawing and description of the modified QCM sample holder, a comparison of the modified Sauerbrey factor with the theoretical factor, a description of the control experiments, a figure of the lamps' and sun's spectral flux densities, a summary of the data employed for this study, a discussion of how the photodegradation rate was scaled to atmospheric conditions, efficiency plots for photodegradation, and a plot of the mass percentage lost over a very long irradiation time period (PDF)

■ AUTHOR INFORMATION

Corresponding Author

*Phone: +1-949-824-1262. Fax: +1-949-824-8671. E-mail: nizkorod@uci.edu.

ORCID

Kurtis T. Malecha: 0000-0002-1438-7440

Sergey A. Nizkorodov: 0000-0003-0891-0052

Notes

The authors declare no competing financial interest.

■ ACKNOWLEDGMENTS

K.T.M. thanks the National Science Foundation (NSF) for support from the Graduate Research Fellowship Program. The PTR-ToF-MS was acquired with NSF Grant MRI-0923323.

■ REFERENCES

(1) Hallquist, M.; Wenger, J. C.; Baltensperger, U.; Rudich, Y.; Simpson, D.; Claeys, M.; Dommen, J.; Donahue, N. M.; George, C.; Goldstein, A. H.; Hamilton, J. F.; Herrmann, H.; Hoffmann, T.; Iinuma, Y.; Jang, M.; Jenkin, M. E.; Jimenez, J. L.; Kiendler-Scharr, A.; Maenhaut, W.; McFiggans, G.; Mentel, T. F.; Monod, A.; Prevot, A. S. H.; Seinfeld, J. H.; Surratt, J. D.; Szmigielski, R.; Wildt, J. The formation, properties and impact of secondary organic aerosol: Current and emerging issues. *Atmos. Chem. Phys.* **2009**, *9*, 5155−5236.

(2) Intergovernmental Panel on Climate Change. *Climate change 2013: The physical science basis*; Cambridge University Press: Cambridge, U.K., 2014.

(3) Malecha, K. T.; Nizkorodov, S. A. Photodegradation of secondary organic aerosol particles as a source of small, oxygenated volatile organic compounds. *Environ. Sci. Technol.* **2016**, *50*, 9990−9997.

(4) George, C.; Ammann, M.; D'Anna, B.; Donaldson, D. J.; Nizkorodov, S. A. Heterogeneous photochemistry in the atmosphere. *Chem. Rev.* **2015**, *115*, 4218−4258.

(5) Shiraiwa, M.; Yee, L. D.; Schilling, K. A.; Loza, C. L.; Craven, J. S.; Zuend, A.; Ziemann, P. J.; Seinfeld, J. H. Size distribution dynamics reveal particle-phase chemistry in organic aerosol formation. *Proc. Natl. Acad. Sci. U. S. A.* **2013**, *110*, 11746−11750.

(6) Henry, K. M.; Donahue, N. M. Photochemical aging of α-pinene secondary organic aerosol: Effects of OH radical sources and photolysis. *J. Phys. Chem. A* **2012**, *116*, 5932−5940.

(7) Epstein, S. A.; Blair, S. L.; Nizkorodov, S. A. Direct photolysis of α-pinene ozonolysis secondary organic aerosol: Effect on particle mass and peroxide content. *Environ. Sci. Technol.* **2014**, *48*, 11251−11258.

(8) Wong, J. P.; Zhou, S.; Abbatt, J. P. Changes in secondary organic aerosol composition and mass due to photolysis: Relative humidity dependence. *J. Phys. Chem. A* **2015**, *119*, 4309−4316.

(9) Daumit, K. E.; Carrasquillo, A. J.; Sugrue, R. A.; Kroll, J. H. Effects of condensed-phase oxidants on secondary organic aerosol formation. *J. Phys. Chem. A* **2016**, *120*, 1386−1394.

(10) Hansel, A.; Jordan, A.; Holzinger, R.; Prazeller, P.; Vogel, W.; Lindinger, W. Proton transfer reaction mass spectrometry: On-line trace gas analysis at the ppb level. *Int. J. Mass Spectrom. Ion Processes* **1995**, *149−150*, 609−619.

(11) Kang, E.; Root, M. J.; Toohey, D. W.; Brune, W. H. Introducing the concept of potential aerosol mass (PAM). *Atmos. Chem. Phys.* **2007**, *7*, 5727−5744.

(12) Kroll, J. H.; Lim, C. Y.; Kessler, S. H.; Wilson, K. R. Heterogeneous oxidation of atmospheric organic aerosol: Kinetics of changes to the amount and oxidation state of particle-phase organic carbon. *J. Phys. Chem. A* **2015**, *119*, 10767−10783.

(13) Peng, Z.; Day, D. A.; Stark, H.; Li, R.; Lee-Taylor, J.; Palm, B. B.; Brune, W. H.; Jimenez, J. L. HO_x radical chemistry in oxidation flow reactors with low-pressure mercury lamps systematically examined by modeling. *Atmos. Meas. Tech.* **2015**, *8*, 4863−4890.

(14) Peng, Z.; Day, D. A.; Ortega, A. M.; Palm, B. B.; Hu, W. W.; Stark, H.; Li, R.; Tsigaridis, K.; Brune, W. H.; Jimenez, J. L. Non-OH chemistry in oxidation flow reactors for the study of atmospheric chemistry systematically examined by modeling. *Atmos. Chem. Phys.* **2016**, *16*, 4283−4305.

(15) Liu, P.; Li, Y. J.; Wang, Y.; Gilles, M. K.; Zaveri, R. A.; Bertram, A. K.; Martin, S. T. Lability of secondary organic particulate matter. *Proc. Natl. Acad. Sci. U. S. A.* **2016**, *113*, 12643−12648.

(16) Grant, J. S.; Shaw, S. K. A model system to mimic environmentally active surface film roughness and hydrophobicity. *Chemosphere* **2017**, *185*, 772−779.

(17) Thomas, E.; Rudich, Y.; Trakhtenberg, S.; Ussyshkin, R. Water adsorption by hydrophobic organic surfaces: Experimental evidence and implications to the atmospheric properties of organic aerosols. *J. Geophys. Res.: Atmos.* **1999**, *104*, 16053−16059.

(18) Rudich, Y.; Benjamin, I.; Naaman, R.; Thomas, E.; Trakhtenberg, S.; Ussyshkin, R. Wetting of hydrophobic organic surfaces and its implications to organic aerosols in the atmosphere. *J. Phys. Chem. A* **2000**, *104*, 5238−5245.

(19) Demou, E.; Visram, H.; Donaldson, D. J.; Makar, P. A. Uptake of water by organic films: The dependence on the film oxidation state. *Atmos. Environ.* **2003**, *37*, 3529−3537.
(20) Molina, M. J.; Ivanov, A. V.; Trakhtenberg, S.; Molina, L. T. Atmospheric evolution of organic aerosol. *Geophys. Res. Lett.* **2004**, *31*, L020910.
(21) Monge, M. E.; Rosenorn, T.; Favez, O.; Muller, M.; Adler, G.; Abo Riziq, A.; Rudich, Y.; Herrmann, H.; George, C.; D'Anna, B. Alternative pathway for atmospheric particles growth. *Proc. Natl. Acad. Sci. U. S. A.* **2012**, *109*, 6840−6844.
(22) Romonosky, D. E.; Laskin, A.; Laskin, J.; Nizkorodov, S. A. High-resolution mass spectrometry and molecular characterization of aqueous photochemistry products of common types of secondary organic aerosols. *J. Phys. Chem. A* **2015**, *119*, 2594−2606.
(23) Sauerbrey, G. Verwendung von schwingquarzen zur wägung dünner schichten und zur mikrowägung. *Eur. Phys. J. A* **1959**, *155*, 206−222.
(24) Calvert, J. A.; Pitts, J. N. *Photochemistry*; John Wiley: New York, 1966.
(25) Malecha, K. T.; Nizkorodov, S. A. Feasibility of photosensitized reactions with secondary organic aerosol particles in the presence of volatile organic compounds. *J. Phys. Chem. A* **2017**, *121*, 4961−4967.
(26) Li, R.; Palm, B. B.; Ortega, A. M.; Hlywiak, J.; Hu, W.; Peng, Z.; Day, D. A.; Knote, C.; Brune, W. H.; de Gouw, J. A.; Jimenez, J. L. Modeling the radical chemistry in an oxidation flow reactor: Radical formation and recycling, sensitivities, and the OH exposure estimation equation. *J. Phys. Chem. A* **2015**, *119*, 4418−4432.
(27) Finlayson-Pitts, B. J.; Pitts, J. N. *Chemistry of the upper and lower atmosphere theory, experiments, and applications*; Academic Press: San Diego, 2000.
(28) Mang, S. A.; Henricksen, D. K.; Bateman, A. P.; Andersen, M. P.; Blake, D. R.; Nizkorodov, S. A. Contribution of carbonyl photochemistry to aging of atmospheric secondary organic aerosol. *J. Phys. Chem. A* **2008**, *112*, 8337−8344.
(29) Borduas, N.; Abbatt, J.; Murphy, J. Gas phase oxidation of monoethanolamine (MEA) with OH radical and ozone: Kinetics, products, and particles. *Environ. Sci. Technol.* **2013**, *47*, 6377−6383.
(30) Romonosky, D. E.; Ali, N. N.; Saiduddin, M. N.; Wu, M.; Lee, H. J.; Aiona, P. K.; Nizkorodov, S. A. Effective absorption cross sections and photolysis rates of anthropogenic and biogenic secondary organic aerosols. *Atmos. Environ.* **2016**, *130*, 172−179.
(31) Chhabra, P. S.; Ng, N. L.; Canagaratna, M. R.; Corrigan, A. L.; Russell, L. M.; Worsnop, D. R.; Flagan, R. C.; Seinfeld, J. H. Elemental composition and oxidation of chamber organic aerosol. *Atmos. Chem. Phys.* **2011**, *11*, 8827−8845.
(32) Lauraguais, A.; Coeur-Tourneur, C.; Cassez, A.; Deboudt, K.; Fourmentin, M.; Choel, M. Atmospheric reactivity of hydroxyl radicals with guaiacol (2-methoxyphenol), a biomass burning emitted compound: Secondary organic aerosol formation and gas-phase oxidation products. *Atmos. Environ.* **2014**, *86*, 155−163.
(33) Kitanovski, Z.; Cusak, A.; Grgic, I.; Claeys, M. Chemical characterization of the main products formed through aqueous-phase photonitration of guaiacol. *Atmos. Meas. Tech.* **2014**, *7*, 2457−2470.
(34) Sangwan, M.; Zhu, L. Absorption cross sections of 2-nitrophenol in the 295−400 nm region and photolysis of 2-nitrophenol at 308 and 351 nm. *J. Phys. Chem. A* **2016**, *120*, 9958−9967.
(35) Barsotti, F.; Bartels-Rausch, T.; De Laurentiis, E.; Ammann, M.; Brigante, M.; Mailhot, G.; Maurino, V.; Minero, C.; Vione, D. Photochemical formation of nitrite and nitrous acid (HONO) upon irradiation of nitrophenols in aqueous solution and in viscous secondary organic aerosol proxy. *Environ. Sci. Technol.* **2017**, *51*, 7486−7495.
(36) Grygoryeva, K.; Kubecka, J.; Pysanenko, A.; Lengyel, J.; Slavicek, P.; Farnik, M. Photochemistry of nitrophenol molecules and clusters: Intra- vs intermolecular hydrogen bond dynamics. *J. Phys. Chem. A* **2016**, *120*, 4139−4146.
(37) Ortega, A. M.; Hayes, P. L.; Peng, Z.; Palm, B. B.; Hu, W.; Day, D. A.; Li, R.; Cubison, M. J.; Brune, W. H.; Graus, M.; Warneke, C.; Gilman, J. B.; Kuster, W. C.; de Gouw, J.; Gutiérrez-Montes, C.; Jimenez, J. L. Real-time measurements of secondary organic aerosol formation and aging from ambient air in an oxidation flow reactor in the Los Angeles area. *Atmos. Chem. Phys.* **2016**, *16*, 7411−7433.
(38) Smith, J.; Dunn, M.; VanReken, T. M.; Iida, K.; Stolzenburg, M.; McMurry, P. H.; Huey, G. Chemical composition of atmospheric nanoparticles formed from nucleation in tecamac, Mexico: Evidence for an important role for organic species in nanoparticle growth. *Geophys. Res. Lett.* **2008**, *35*, L04808.
(39) Hodzic, A.; Madronich, S.; Kasibhatla, P. S.; Tyndall, G.; Aumont, B.; Jimenez, J. L.; Lee-Taylor, J.; Orlando, J. Organic photolysis reactions in tropospheric aerosols: Effect on secondary organic aerosol formation and lifetime. *Atmos. Chem. Phys.* **2015**, *15*, 9253−9269.
(40) Yu, P.; Rosenlof, K. H.; Liu, S.; Telg, H.; Thornberry, T. D.; Rollins, A. W.; Portmann, R. W.; Bai, Z.; Ray, E. A.; Duan, Y.; Pan, L. L.; Toon, O. B.; Bian, J.; Gao, R. S. Efficient transport of tropospheric aerosol into the stratosphere via the asian summer monsoon anticyclone. *Proc. Natl. Acad. Sci. U. S. A.* **2017**, *114*, 6972−6977.
(41) Shiraiwa, M.; Li, Y.; Tsimpidi, A. P.; Karydis, V. A.; Berkemeier, T.; Pandis, S. N.; Lelieveld, J.; Koop, T.; Poschl, U. Global distribution of particle phase state in atmospheric secondary organic aerosols. *Nat. Commun.* **2017**, *8*, 15002.
(42) Murphy, D. M.; Cziczo, D. J.; Hudson, P. K.; Thomson, D. S. Carbonaceous material in aerosol particles in the lower stratosphere and tropopause region. *J. Geophys. Res.* **2007**, *112*, D04203.

DOI: 10.1021/acs.estlett.8b00231
Environ. Sci. Technol. Lett. 2018, 5, 366−371